Periodic Outbreaks in Compartmental Epidemic Models

Jinghao Chen[a]

[a] University of Science and Technology of China, No. 96 Jinzhai Road, Baohe District, Hefei, 230026, Anhui, China

ARTICLE INFO

Keywords:
SIR Model
Periodic Outbreaks
Demographics
Seasonal Forcing
Early Fade-out

ABSTRACT

This report studies the mechanisms by which recurrent epidemic outbreaks may arise from susceptible–infected–removed (SIR)-type differential equation models. Starting from the basic SIR model, the experiments first show why a closed susceptible–infected–removed system produces a single outbreak and then approaches disease disappearance. The model is then extended by balanced births and deaths, which replenish susceptible individuals and allow secondary infection peaks after the initial epidemic wave. A seasonally forced transmission rate is further introduced to test whether an external periodic driver can maintain long-term recurrent outbreaks. Finally, an integer-population stochastic model is used to examine early fade-out when the number of infected individuals is small. The numerical results form a consistent mechanism chain: the basic SIR model explains a single epidemic, demographic turnover provides a susceptible source for recurrent peaks, seasonal forcing sustains richer long-term periodic structures, and stochasticity can prevent outbreak establishment even when the deterministic model predicts growth.

1. Introduction

Many infectious diseases do not simply rise once and then disappear immediately from observation. Instead, infection curves may display repeated waves, changing peak intervals, and occasional failure to establish when the number of infected individuals is small. The central modeling question in this report is therefore the following: what is the minimal mechanism that can explain sustained recurrent outbreaks beyond a single epidemic wave?

The study is organized as a sequence of increasingly expressive epidemic models. The first part considers a basic susceptible–infected–removed (SIR) model without new susceptible input. This model is useful for explaining the threshold condition for outbreak growth and the depletion mechanism that causes the epidemic to end. The second part adds balanced births and deaths. This extension does not introduce an explicit periodic driver, but it continually returns removed individuals to the susceptible class through population turnover, so secondary peaks may appear. The third part introduces a time-dependent transmission rate with annual periodicity. This seasonal forcing acts as an external driver and can generate long-term recurrent patterns after transient dynamics are removed. The fourth part replaces the continuous infected proportion by integer counts and simulates stochastic event sequences, which is necessary for studying early fade-out when infected counts are small.

The goal is not to fit real epidemic data, but to isolate the qualitative mechanisms behind periodic outbreak formation. The experiments therefore compare deterministic trajectories, threshold scans, demographic recurrent peaks, seasonal alpha scans, and repeated stochastic simulations under controlled parameter settings. All conclusions in the report are based on the generated numerical outputs and the displayed figures. The experimental design also separates three ideas that are easily confused in qualitative discussions: the occurrence of one large epidemic peak, the recurrence of later peaks through susceptible replenishment, and the maintenance of externally organized periodicity under time-varying transmission. This separation makes it possible to identify which modeling assumption is responsible for each observed behavior rather than attributing all repeated waves to a single mechanism.

Figure 1 summarizes the overall experimental workflow. The framework begins with the baseline SIR mechanism, then adds demographic replenishment and seasonal forcing to explain recurrent outbreaks, and finally uses stochastic simulation to test finite-population fade-out. This organization matches the sequence of modeling assumptions and numerical experiments used throughout the report.

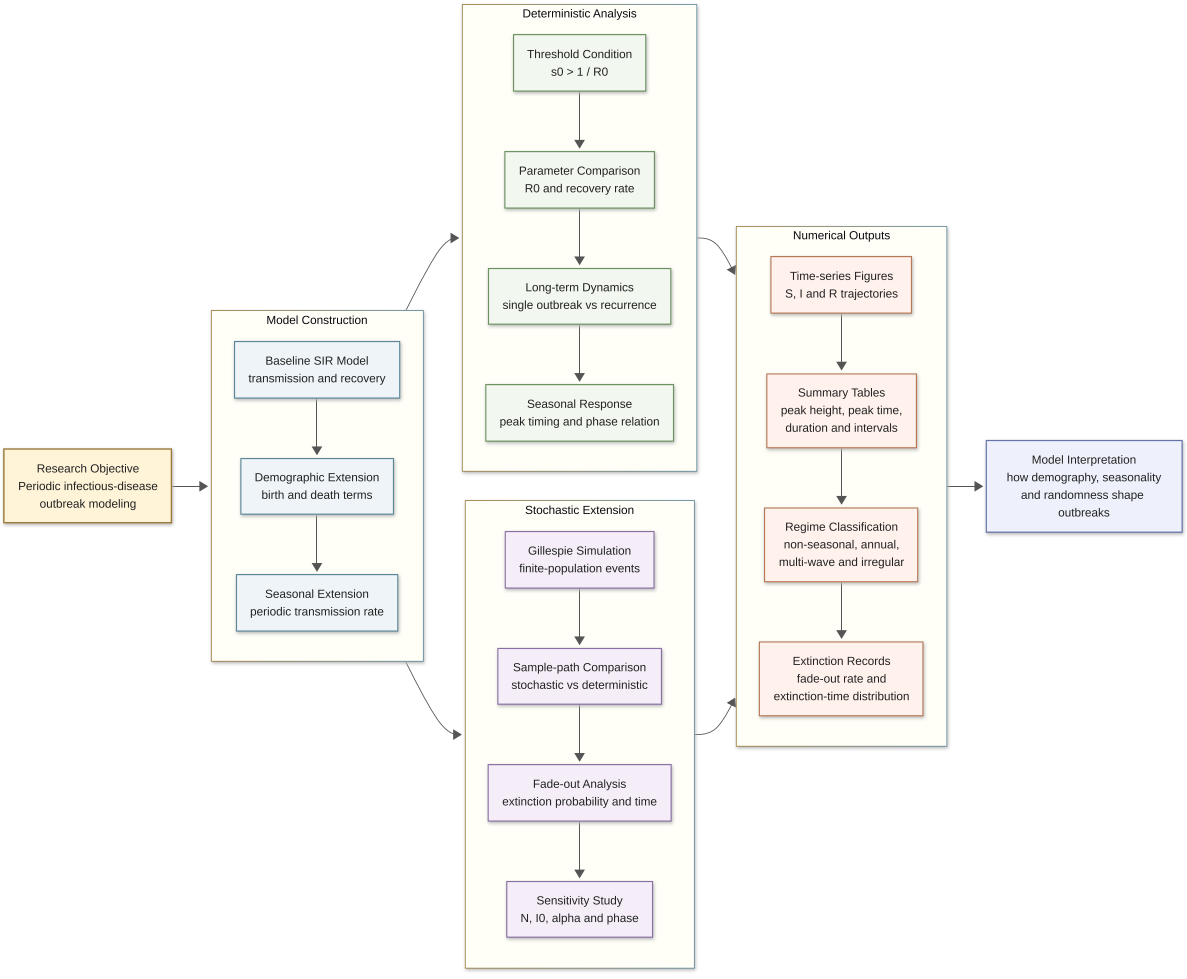

Figure 1: Overall workflow of the periodic infectious-disease outbreak modeling experiment.

2. Mathematical Models

2.1. Parameter choices and epidemiological ranges

All numerical parameters in this report are chosen as representative epidemiological values rather than as a direct calibration to a single real outbreak. The time unit is one year. The recovery parameter is fixed at $\gamma = 52\,\mathrm{yr}^{-1}$, so the mean infectious period is

$$\frac{1}{\gamma} = \frac{1}{52}\ \mathrm{yr} \approx 7.0\ \mathrm{days}. \tag{1}$$

This one-week scale is consistent with several common acute infections. For example, the CDC states that mumps patients are considered infectious from two days before to five days after parotitis onset, and that measles is infectious from four days before to four days after rash onset.[1,2]

The tested reproduction numbers $R_0 = 2, 8, 15$ are used to span low, intermediate, and high transmissibility regimes. A systematic review of influenza reproduction numbers reports median values around 1.28 for seasonal influenza and 1.46 for the 2009 pandemic, which supports using $R_0 = 2$ as a low-to-moderate transmission case.[3] For

[1] CDC, Clinical Overview of Mumps: https://www.cdc.gov/mumps/hcp/clinical-overview/index.html

[2] CDC, Measles Clinical Diagnosis Fact Sheet: https://www.cdc.gov/measles/hcp/communication-resources/clinical-diagnosis-fact-sheet.html

[3] Biggerstaff et al., *BMC Infectious Diseases* 2014: https://pmc.ncbi.nlm.nih.gov/articles/PMC4169819/

childhood infections with stronger transmission, varicella is commonly associated with a basic reproduction number around 8–10, while measles is often cited around 12–18.[4,5] Thus the values $2, 8, 15$ are not disease labels, but a controlled range that covers weak, moderate, and highly contagious epidemic regimes.

For the demographic model, $\mu = 1/70\ \mathrm{yr}^{-1}$ corresponds to an average demographic lifetime of about 70 years. This is a standard order-of-magnitude choice for human-population turnover and is consistent with global life-expectancy data being on the scale of several decades.[6] Finally, the seasonal form $\beta(t) = \beta_0[1 + \alpha\cos(2\pi t + \phi)]$ is an idealized representation of periodic variation in transmission. Seasonal forcing is widely used in infectious-disease modeling to study recurrent outbreaks and calendar-driven variation in incidence.[7] Therefore the α-scan in this report should be interpreted as a mechanism experiment on forcing strength, rather than as a fitted estimate for one specific disease.

2.2. Basic SIR model

The deterministic variables are normalized population proportions

$$s(t) = \frac{S(t)}{N}, \qquad i(t) = \frac{I(t)}{N}, \qquad r(t) = \frac{R(t)}{N}, \tag{2}$$

so that ideally $s(t) + i(t) + r(t) = 1$. In the basic SIR model, susceptible individuals are infected through contact with infected individuals, and infected individuals recover into the removed class. The equations are

$$\frac{\mathrm{d}s}{\mathrm{d}t} = -\beta si, \tag{3}$$

$$\frac{\mathrm{d}i}{\mathrm{d}t} = \beta si - \gamma i, \tag{4}$$

$$\frac{\mathrm{d}r}{\mathrm{d}t} = \gamma i. \tag{5}$$

Here β is the transmission rate and γ is the recovery rate. The infection term βsi transfers individuals from the susceptible class to the infected class, while γi transfers infected individuals to the removed class.

Adding the three equations gives

$$\frac{\mathrm{d}}{\mathrm{d}t}(s + i + r) = 0, \tag{6}$$

so the simplex $s + i + r = 1$ is invariant for normalized initial data. Moreover,

$$\frac{\mathrm{d}s}{\mathrm{d}t} \le 0, \qquad \frac{\mathrm{d}r}{\mathrm{d}t} \ge 0, \tag{7}$$

which means that the susceptible class is monotonically depleted and the removed class is monotonically accumulated. These two monotonicity properties are the mathematical reason why the basic model can produce a large first wave but cannot restore the conditions for a second wave.

The instantaneous growth of infection is determined by

$$\frac{\mathrm{d}i}{\mathrm{d}t} = i(\beta s - \gamma). \tag{8}$$

It is useful to define the effective reproduction factor at time t as

$$\mathcal{R}_{\mathrm{eff}}(t) = \frac{\beta s(t)}{\gamma} = R_0 s(t), \qquad R_0 = \frac{\beta}{\gamma}. \tag{9}$$

When $i(t) > 0$, infection increases exactly when

$$\mathcal{R}_{\mathrm{eff}}(t) > 1 \qquad \Longleftrightarrow \qquad s(t) > \frac{\gamma}{\beta} = \frac{1}{R_0}. \tag{10}$$

[4] Otani et al., *Viruses* 2022, varicella epidemiology: `https://pmc.ncbi.nlm.nih.gov/articles/PMC8954496/`

[5] Guerra et al., *The Lancet Infectious Diseases* 2017, measles R_0 review: `https://pubmed.ncbi.nlm.nih.gov/28757186/`

[6] World Bank, Life expectancy at birth, total years: `https://data.worldbank.org/indicator/SP.DYN.LE00.IN`

[7] Grassly and Fraser, *Proceedings of the Royal Society B* 2006: `https://pmc.ncbi.nlm.nih.gov/articles/PMC1634916/`

Therefore the infection peak occurs, in the continuous deterministic model, near the crossing condition

$$s(t_{\text{peak}}) = \frac{1}{R_0}, \qquad \frac{\mathrm{d}i}{\mathrm{d}t}(t_{\text{peak}}) = 0. \tag{11}$$

This is a local growth condition: it explains the initial direction of the infected curve and the location of the peak, but it does not by itself imply long-term persistence. Once the outbreak has consumed enough susceptible individuals, $\mathcal{R}_{\text{eff}}(t)$ falls below one, and recovery dominates transmission.

A second useful identity follows by dividing the removed equation by the susceptible equation:

$$\frac{\mathrm{d}r}{\mathrm{d}s} = \frac{\gamma i}{-\beta s i} = -\frac{1}{R_0 s}. \tag{12}$$

After integration, one obtains the invariant relation

$$r(t) - r_0 = -\frac{1}{R_0} \log \frac{s(t)}{s_0}, \qquad \text{or equivalently} \qquad \log s(t) + R_0 r(t) = \log s_0 + R_0 r_0. \tag{13}$$

If $i(t) \to 0$ as $t \to \infty$, the final susceptible proportion s_∞ satisfies the final-size equation

$$r_\infty - r_0 = s_0 + i_0 - s_\infty, \qquad \log \frac{s_\infty}{s_0} = -R_0(r_\infty - r_0). \tag{14}$$

The exact numerical value of s_∞ is determined implicitly, but the qualitative implication is direct: the epidemic ends because the susceptible pool has been driven below the growth threshold. Thus $i(t)$ approaches zero in the long run, while $r(t)$ accumulates the individuals who have passed through infection.

2.3. SIR model with demographic dynamics

To allow the susceptible pool to be replenished, balanced births and deaths are added. In normalized variables, the demographic SIR model is

$$\frac{\mathrm{d}s}{\mathrm{d}t} = \mu - \beta_0 s i - \mu s, \tag{15}$$

$$\frac{\mathrm{d}i}{\mathrm{d}t} = \beta_0 s i - \gamma i - \mu i, \tag{16}$$

$$\frac{\mathrm{d}r}{\mathrm{d}t} = \gamma i - \mu r. \tag{17}$$

The parameter μ is the natural turnover rate. The term μ represents births into the susceptible class, while $-\mu s$, $-\mu i$, and $-\mu r$ represent natural deaths from the three compartments. Since births and deaths are balanced at the population level, the total normalized population remains close to one.

Again, summing the equations gives

$$\frac{\mathrm{d}}{\mathrm{d}t}(s + i + r) = \mu\{1 - (s + i + r)\}, \tag{18}$$

so the plane $s + i + r = 1$ is invariant and attractive. The disease-free state is

$$E_0 = (1, 0, 0). \tag{19}$$

Linearizing the infected equation near E_0 gives

$$\frac{\mathrm{d}i}{\mathrm{d}t} \approx i\{\beta_0 - (\gamma + \mu)\}. \tag{20}$$

Thus the demographic reproduction number is

$$R_0 = \frac{\beta_0}{\gamma + \mu}, \tag{21}$$

with outbreak growth near the disease-free state when $R_0 > 1$. For $R_0 > 1$, the endemic equilibrium is obtained from $\mathrm{d}i/\mathrm{d}t = 0$ and $\mathrm{d}s/\mathrm{d}t = 0$:

$$s^* = \frac{\gamma + \mu}{\beta_0} = \frac{1}{R_0}, \qquad i^* = \frac{\mu(1 - s^*)}{\gamma + \mu} = \frac{\mu(R_0 - 1)}{\beta_0}, \qquad r^* = \frac{\gamma}{\mu} i^*. \tag{22}$$

This equilibrium formula explains why demographic turnover changes the long-term interpretation: the model no longer forces the infected proportion to vanish solely because the susceptible class has been depleted. Births gradually restore susceptible individuals and can maintain a positive endemic level or generate recurrent approaches toward that level.

The local oscillatory mechanism can also be seen from the two-dimensional subsystem for (s, i) on $s + i + r = 1$. At the endemic equilibrium, the Jacobian matrix is

$$J_* = \begin{pmatrix} -\mu R_0 & -(\gamma + \mu) \\ \mu(R_0 - 1) & 0 \end{pmatrix}. \tag{23}$$

Its trace and determinant are

$$\mathrm{tr}(J_*) = -\mu R_0 < 0, \qquad \det(J_*) = \mu(\gamma + \mu)(R_0 - 1) > 0. \tag{24}$$

For the high-transmission settings used in the experiments, these quantities are consistent with stable return toward the endemic state, often through damped oscillatory transients. Compared with the basic SIR model, the important new mechanism is therefore susceptible replenishment. Even after a large initial outbreak, demographic turnover can gradually increase $s(t)$ again; once the susceptible level becomes large enough, a later outbreak can occur. With constant transmission, this mechanism often produces damped recurrent peaks or convergence toward an endemic state rather than externally maintained complex periodic motion.

2.4. Seasonally forced SIR model

Seasonality is introduced by replacing the constant transmission rate with

$$\beta(t) = \beta_0 \left(1 + \alpha \cos(2\pi t)\right), \tag{25}$$

where time is measured in years. The parameter β_0 is the mean transmission rate and $\alpha \in [0, 1]$ controls the seasonal forcing strength. When $\alpha = 0$, the model reduces to the demographic SIR model with constant transmission. Larger α produces stronger annual variation in transmission.

The resulting model is

$$\frac{\mathrm{d}s}{\mathrm{d}t} = \mu - \beta(t) s i - \mu s, \tag{26}$$

$$\frac{\mathrm{d}i}{\mathrm{d}t} = \beta(t) s i - \gamma i - \mu i, \tag{27}$$

$$\frac{\mathrm{d}r}{\mathrm{d}t} = \gamma i - \mu r. \tag{28}$$

This model contains both susceptible replenishment and an external periodic driver. The instantaneous effective reproduction factor becomes

$$\mathcal{R}_{\mathrm{eff}}(t) = \frac{\beta(t) s(t)}{\gamma + \mu} = R_0 \{1 + \alpha \cos(2\pi t)\} s(t), \qquad R_0 = \frac{\beta_0}{\gamma + \mu}. \tag{29}$$

Therefore infection grows at time t precisely when

$$\mathcal{R}_{\mathrm{eff}}(t) > 1 \qquad \Longleftrightarrow \qquad s(t) > \frac{1}{R_0 \{1 + \alpha \cos(2\pi t)\}}. \tag{30}$$

This inequality shows why the seasonal model can produce phase-shifted outbreaks. A high-transmission season lowers the susceptible threshold for growth, but a large outbreak still requires enough susceptible individuals to have accumulated before or during that favorable part of the year.

Because $\beta(t)$ has period one year, the long-run dynamics can be diagnosed by annual sampling. If $x(t) = (s(t), i(t), r(t))$, the annual map is

$$P : x(n) \mapsto x(n+1), \tag{31}$$

where n is an integer year. A stable annual cycle would appear as nearly one repeated point in the sampled infected values, while a multi-year cycle would appear as several repeated annual levels. More dispersed annual samples suggest irregular or complex long-run behavior over the finite simulation window. Peak statistics provide a complementary description. If detected peaks occur at times $t_1, t_2, \dots, t_m$ with peak infected proportions $p_1, p_2, \dots, p_m$, then the mean peak height and mean peak interval are

$$\bar{p} = \frac{1}{m}\sum_{k=1}^{m} p_k, \qquad \bar{\Delta} = \frac{1}{m-1}\sum_{k=1}^{m-1}(t_{k+1} - t_k). \tag{32}$$

The coefficient of variation used in the tables is

$$\mathrm{CV}(p) = \frac{\sqrt{(m-1)^{-1}\sum_{k=1}^{m}(p_k - \bar{p})^2}}{\bar{p}}, \qquad \mathrm{CV}(\Delta) = \frac{\sqrt{(m-1)^{-1}\sum_{k=1}^{m-1}(\Delta_k - \bar{\Delta})^2}}{\bar{\Delta}}. \tag{33}$$

These quantities are numerical diagnostics rather than a formal bifurcation theorem, but they are appropriate for comparing how forcing strength changes long-term outbreak regularity. The numerical experiments therefore simulate a long time interval and then remove the transient stage to focus on the long-term structure of $i(t)$. This choice is important because the first outbreak can be large even without sustained periodicity; the later part of the trajectory is the relevant evidence for whether a periodic outbreak mechanism remains active after the initial depletion event.

2.5. Stochastic Gillespie model

The stochastic experiments use integer counts (S, I, R) with fixed population size N. At any time t, the possible events are infection, recovery, infected death with susceptible replacement, and recovered death with susceptible replacement. Their event rates are

$$S + I \longrightarrow 2I, \qquad a_1(t) = \beta(t)\frac{SI}{N}, \tag{34}$$

$$I \longrightarrow R, \qquad a_2(t) = \gamma I, \tag{35}$$

$$I \longrightarrow S, \qquad a_3(t) = \mu I, \tag{36}$$

$$R \longrightarrow S, \qquad a_4(t) = \mu R. \tag{37}$$

A susceptible death immediately followed by susceptible replacement does not change the state and is therefore omitted from the event list. The total event rate is

$$a_0(t) = a_1(t) + a_2(t) + a_3(t) + a_4(t). \tag{38}$$

Conditioned on an event occurring at the current state, the probability that event k occurs is

$$\mathbb{P}(\text{event } k \mid S, I, R, t) = \frac{a_k(t)}{a_0(t)}, \qquad k = 1, 2, 3, 4. \tag{39}$$

For a small time interval Δt, the event approximation is

$$\mathbb{P}(\text{one event of type } k \text{ in } [t, t+\Delta t]) = a_k(t)\Delta t + o(\Delta t), \tag{40}$$

which connects the stochastic event rates with the deterministic mean-field equations. If the population size is large and the proportions are $s = S/N$, $i = I/N$, and $r = R/N$, the expected drift of the stochastic process has the same compartmental form as the deterministic demographic or seasonal equations.

The key difference is the absorbing boundary

$$I = 0. \tag{41}$$

Once the process reaches this boundary, there are no infected individuals left to create new infection events, so infection cannot restart without external introduction. To formalize establishment, define the hitting times

$$\tau_0 = \inf\{t : I(t) = 0\}, \qquad \tau_M = \inf\{t : I(t) \geq M\}, \tag{42}$$

where M is the major-outbreak threshold used in the experiment. A major outbreak is the event

$$\tau_M < \tau_0, \tag{43}$$

while early fade-out is the complementary failure of establishment before reaching the threshold,

$$\tau_0 < \tau_M \quad \text{or failure to reach } M \text{ within the simulation window.} \tag{44}$$

The empirical probabilities reported later are therefore

$$\widehat{P}_{\text{fade}} = \frac{\#\{\text{early fade-out runs}\}}{\#\{\text{all repeated runs}\}}, \qquad \widehat{P}_{\text{major}} = 1 - \widehat{P}_{\text{fade}}. \tag{45}$$

Thus the reported early fade-out probability is not interpreted as a final extinction probability after a fully established epidemic; it measures failure of establishment from a small initial infected count.

3. Numerical Methods and Experimental Design

The deterministic systems are solved with a fourth-order Runge–Kutta method. For an ordinary differential equation $y' = f(t, y)$ with time step h, one step has the form

$$\begin{aligned} k_1 &= f(t_n, y_n), \\ k_2 &= f\left(t_n + \frac{h}{2}, y_n + \frac{h}{2}k_1\right), \\ k_3 &= f\left(t_n + \frac{h}{2}, y_n + \frac{h}{2}k_2\right), \\ k_4 &= f(t_n + h, y_n + hk_3), \\ y_{n+1} &= y_n + \frac{h}{6}(k_1 + 2k_2 + 2k_3 + k_4). \end{aligned} \tag{46}$$

This numerical method is used because the deterministic models are smooth systems and because the seasonal model requires resolving a time-dependent transmission coefficient. The time unit in the equations is one year. For short initial outbreaks, the horizontal axis is often shown in days to make the rapid epidemic wave easier to read. For demographic and seasonal experiments, years are retained because recurrent peaks occur on longer time scales.

The main parameter and experiment settings are summarized in Table 1. The recovery rate is $\gamma = 52\,\text{yr}^{-1}$ in the baseline setting, corresponding to a mean infectious period of about 7.02 days. Demographic turnover uses $\mu = 1/70\,\text{yr}^{-1}$. The basic SIR comparison uses $R_0 = 2, 8, 15$, while the demographic and seasonal main experiments emphasize a high-transmission regime with $R_0 = 15$. The seasonal alpha scan covers $0 \leq \alpha \leq 0.8$ and uses long simulations so that transient effects can be discarded.

Table 1
Main parameter settings used in the deterministic and stochastic experiments. The values are rounded from the numerical experiment settings and outputs.

Quantity	Value	Role in the experiments
Baseline recovery rate γ	$52\,\mathrm{yr}^{-1}$	Mean infectious period about 7.02 days.
Demographic turnover rate μ	$1/70 \approx 0.0143\,\mathrm{yr}^{-1}$	Balanced births and natural deaths.
Initial deterministic state	$(s_0, i_0, r_0) = (0.9999, 10^{-4}, 0)$	Baseline normalized initial condition.
Basic SIR R_0 values	$2, 8, 15$	Low, moderate, and high transmission regimes.
Basic SIR β values	$104, 416, 780\,\mathrm{yr}^{-1}$	Computed from $\beta = R_0\gamma$.
Main demographic R_0	15	High-transmission demographic experiment.
Main demographic β_0	$780.214\,\mathrm{yr}^{-1}$	Computed from $\beta_0 = R_0(\gamma + \mu)$.
Seasonal alpha curves	$0, 0.05, 0.10, 0.20,$ $0.30, 0.40, 0.60$	Representative forcing strengths for long-term curves.
Seasonal alpha scan	0 to 0.8 with 61 values	Annual-sampling diagnostic for long-term patterns.
Stochastic trajectory setting	$N = 10000$, $I_0 = 20$, 30 repeats	Visual comparison with the deterministic outbreak curve.
Stochastic establishment scan	$N = 1000, 3000, 10000, 30000$; $I_0 = 1, 2, 5, 10$; 100 repeats	Near-threshold early fade-out and major-outbreak probability.
Major-outbreak threshold	near $0.005N$	Establishment threshold used to separate early fade-out from major outbreak establishment.
Seasonal stochastic alpha scan	$N = 10000$, $I_0 = 5$, $\alpha = 0, 0.1, 0.3, 0.6$	Early fade-out under phase-0 seasonal initialization.

Peak detection is used to summarize recurrent outbreaks after transient removal. For the seasonal scan, annual samples of the long-run infected proportion are also recorded. The resulting pattern labels are numerical diagnostics rather than strict bifurcation proofs. In the stochastic experiments, repeated simulations are used to estimate early fade-out probability, major-outbreak probability, and the distribution of fade-out times. The deterministic and stochastic experiments are therefore not intended to answer identical questions. The deterministic curves describe the expected compartment-level tendency under continuous proportions, whereas the stochastic repetitions measure how often a small integer-valued infection seed survives long enough to enter the large-outbreak regime.

4. Results

4.1. Basic SIR: why does a single outbreak end?

Figure 2 shows the baseline basic SIR trajectory and the effect of changing R_0. For $R_0 = 8$, the susceptible proportion decreases rapidly, the infected curve reaches a sharp peak, and the removed class approaches almost the whole population. The comparison across R_0 confirms that larger R_0 produces a faster and higher epidemic peak. However, all three basic SIR curves have only one local infection peak and then decay toward zero.

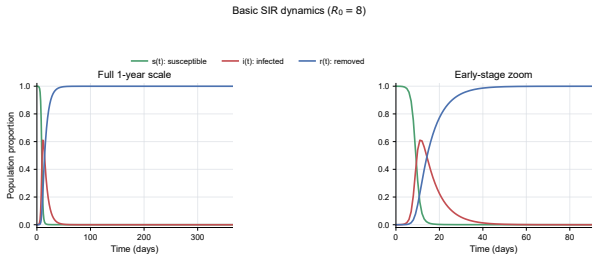

(a) Baseline $R_0 = 8$ dynamics. The single sharp infection wave is followed by depletion of susceptible individuals and disappearance of infection.

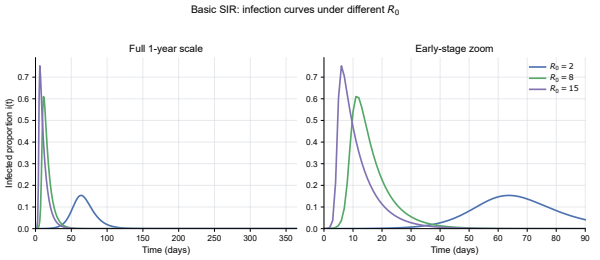

(b) Changing R_0 changes peak height and timing, but each basic SIR trajectory still produces only one major outbreak.

Figure 2: Basic SIR outbreak behavior under the baseline setting and under different reproduction numbers.

The recovery-rate comparison in Figure 3 shows that, at fixed $R_0 = 8$, a larger γ compresses the outbreak into a shorter time window because the mean infectious period is shorter. The threshold scan directly supports the analytic condition $s_0 > 1/R_0$. When $R_0 = 8$, the threshold is $1/R_0 = 0.125$. Below this level, the peak infected proportion remains essentially at the initial value; above it, the outbreak peak increases with the initial susceptible proportion.

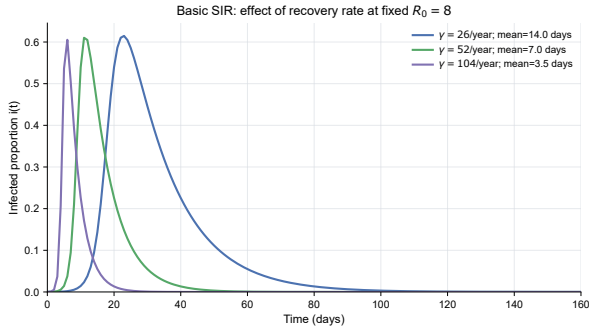

(a) At fixed $R_0 = 8$, faster recovery shifts the epidemic peak earlier and reduces the duration of the high-infection interval.

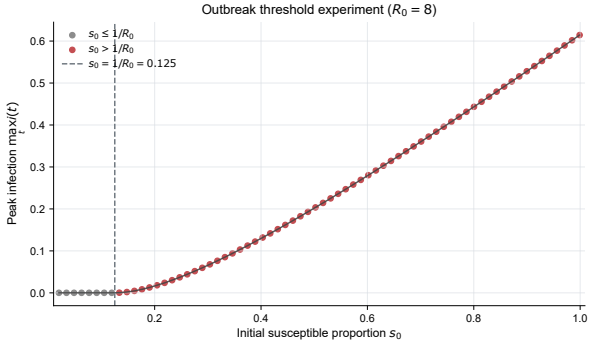

(b) The threshold experiment is consistent with the condition $s_0 > 1/R_0$ for outbreak growth.

Figure 3: Recovery-rate and initial-susceptible threshold effects in the basic SIR model.

Table 2 gives the corresponding numerical summaries. In the R_0 comparison, the peak time decreases from about 63.5 days at $R_0 = 2$ to about 6.0 days at $R_0 = 15$, while the peak infected proportion increases from about 0.153 to 0.752. The final infected value is numerically close to zero in all cases. In the recovery-rate comparison, the peak height remains near 0.61 because R_0 is fixed, but the time to peak and the width at half peak decrease as γ increases.

Table 2
Basic SIR numerical summary. Peak times and widths are reported in days. The width above half peak is reported for the recovery-rate comparison, where it measures the duration for which the infected proportion stays above one half of its peak value.

Series	Setting	β	γ	Peak time	Peak i	Final i	Width above half peak
R_0 comparison	$R_0 = 2$	104	52	63.5	0.153	3.64×10^{-12}	–
R_0 comparison	$R_0 = 8$	416	52	11.5	0.615	1.17×10^{-22}	–
R_0 comparison	$R_0 = 15$	780	52	6.0	0.752	5.10×10^{-23}	–
Recovery comparison	$\gamma = 26$	208	26	23.0	0.615	9.13×10^{-6}	18.0
Recovery comparison	$\gamma = 52$	416	52	11.5	0.615	2.14×10^{-11}	8.5
Recovery comparison	$\gamma = 104$	832	104	5.5	0.609	1.18×10^{-22}	4.0

The numerical threshold behavior is consistent with the analytical sign condition $\mathrm{d}i/\mathrm{d}t = i(\beta s - \gamma)$. In particular, the peak is not controlled only by R_0; it is controlled by the product $R_0 s(t)$. A larger R_0 initially increases $\mathcal{R}_{\mathrm{eff}}(0)$, but it also accelerates the decline of $s(t)$. Once $s(t)$ crosses $1/R_0$, the same mathematical term that produced rapid growth becomes negative and drives the infection curve downward. This explains why increasing transmission intensity changes the timing and magnitude of the first peak without creating sustained recurrence.

These results answer the first modeling question. The basic SIR model can explain why an epidemic wave rises and falls, but it cannot by itself sustain repeated outbreaks because it has no source that restores susceptible individuals after the initial wave. The distinction between peak size and persistence is therefore essential: increasing R_0 makes the first outbreak more intense, but it also depletes susceptible individuals more strongly, so it does not create a mechanism for repeated waves.

4.2. Demographic dynamics: can recurrent outbreaks appear naturally?

Adding demographic turnover changes the long-term mechanism. Figure 4 shows a high-transmission demographic trajectory with $R_0 = 15$. After the initial outbreak, the susceptible population slowly increases again, and the infected curve shows later recurrent peaks. Figure 4b further shows that these late peaks depend strongly on R_0: the $R_0 = 2$ case has no detected late peak, while larger values generate recurrent peaks on a logarithmic infection scale.

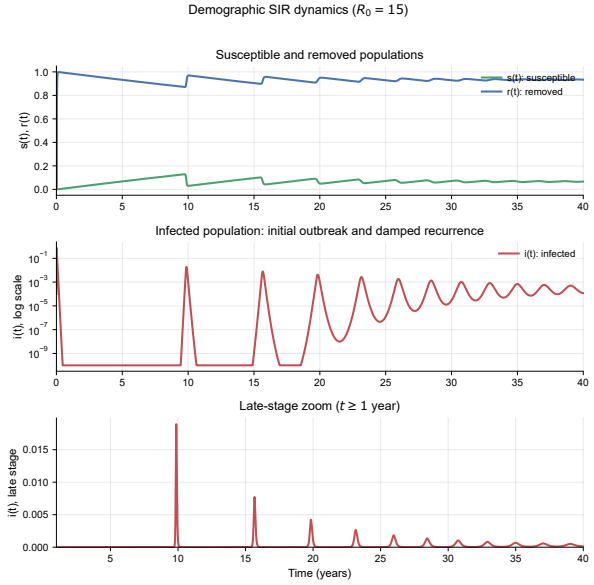

(a) Balanced population turnover replenishes susceptible individuals, allowing late infection peaks after the first outbreak.

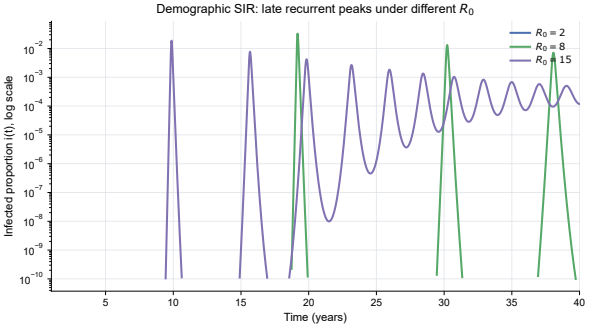

(b) Higher R_0 values lead to more visible recurrent peaks, while $R_0 = 2$ does not produce detected late peaks in this experiment.

Figure 4: Demographic SIR dynamics and their dependence on transmission strength.

The direct comparison in Figure 5 clarifies the difference between the basic and demographic models. This comparison is especially useful because the early epidemic segment is controlled mainly by transmission and recovery, whereas the late segment is controlled by the much slower demographic time scale. Their early outbreak curves are nearly indistinguishable because the outbreak happens on a much shorter time scale than demographic turnover. The long-term behavior is different: the basic SIR infected proportion remains near zero, whereas the demographic model can regenerate infection peaks after susceptible replenishment.

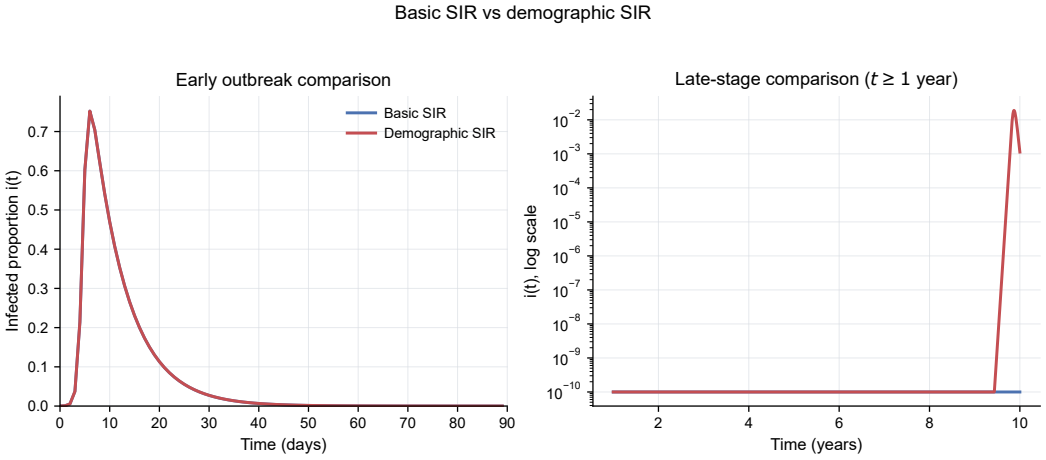

Figure 5: Basic and demographic SIR models are similar during the initial outbreak, but only the demographic model produces late-stage recurrent infection peaks.

Table 3 summarizes the demographic comparison. At $R_0 = 8$, three late peaks are detected after the first year, with the first late peak around year 19.18. At $R_0 = 15$, eleven late peaks are detected after the first year, with the first late peak around year 9.87 and a mean late-peak interval of about 2.92 years. This supports the interpretation that demographic turnover can naturally create recurrent outbreaks, although the constant-transmission model does not provide an external annual driver.

Table 3
Demographic SIR summary under different R_0 values. Late peaks are counted after the first year to separate secondary recurrent behavior from the initial outbreak.

R_0	β_0	Peak time (days)	Peak i	Late peaks	First late peak (yr)	Mean late interval (yr)
2	104.029	63.5	0.154	0	–	–
8	416.114	11.5	0.615	3	19.18	9.44
15	780.214	6.0	0.752	11	9.87	2.92

The late-peak intervals in Table 3 also show that recurrence is not automatically annual. The period is an outcome of the interaction between susceptible replenishment, recovery, and transmission intensity. Mathematically, after the first outbreak reduces $s(t)$ below $1/R_0$, the demographic term $\mu(1 - s)$ slowly pushes $s(t)$ upward again. A later peak becomes possible when the trajectory returns to a region where $\beta_0 s(t) > \gamma + \mu$. This slow-fast contrast explains why the first peak occurs on a days scale, while recurrent demographic peaks occur on a years scale.

Thus, demographic dynamics answer the second modeling question in a qualified way. They can produce recurrent outbreaks because the susceptible pool is replenished, but the observed late peaks are better interpreted as internally generated recurrent or damped behavior rather than a complete explanation of sustained externally synchronized periodic outbreaks.

4.3. Seasonal forcing: can periodic transmission sustain outbreaks?

The seasonal model introduces an explicit annual driver through $\beta(t)$. Figure 6 displays long-run infection curves after transient removal for several forcing strengths. When $\alpha = 0$, the long-run infection level shows small recurrent oscillations. As α increases, the infection response becomes more pulse-like, and the peak timing and peak magnitude change substantially across forcing strengths.

Figure 6: Long-run seasonal infection curves after transient removal. Stronger seasonal forcing produces sharper and more separated infection bursts, indicating that the external periodic driver can organize recurrent outbreaks.

Figure 7 compares the transmission curve with the infection response for $\alpha = 0.30$. The infection peak does not simply coincide with the maximum of $\beta(t)$. Instead, it appears after the seasonal transmission environment and the susceptible level jointly allow rapid growth. This phase relationship is important because recurrent outbreaks depend on both forcing and the internal susceptible–infected state.

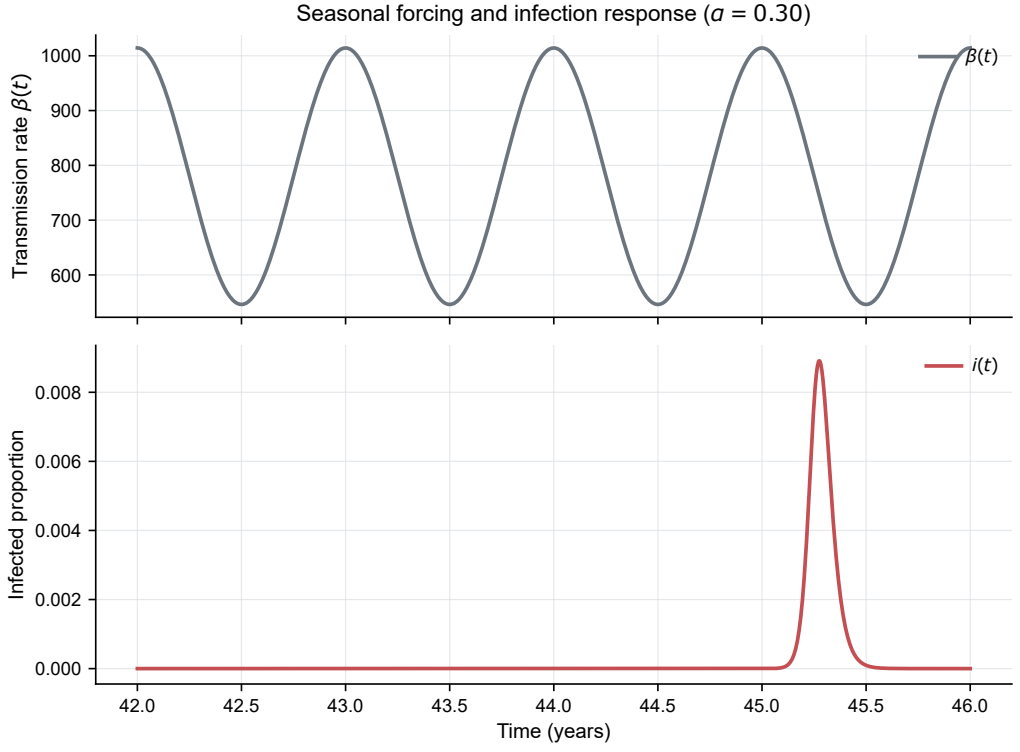

Figure 7: Seasonal transmission and infection response for $\alpha = 0.30$. The infection burst is phase-shifted relative to the transmission wave, showing that outbreaks depend on both external forcing and internal susceptible accumulation.

The alpha scan in Figure 8 gives a broader view of long-run dynamics. The Poincare-style annual sampling plot shows that the long-term annual infection values are concentrated near very small levels for weak forcing, but become more dispersed as forcing increases. The peak-statistics plot shows that both mean peak height and peak interval vary with α. The pattern map gives a compact diagnostic classification: small oscillations dominate near $\alpha = 0$, irregular or complex numerical patterns appear across a wide middle range, and multi-year recurrent peaks appear in parts of the high-forcing range.

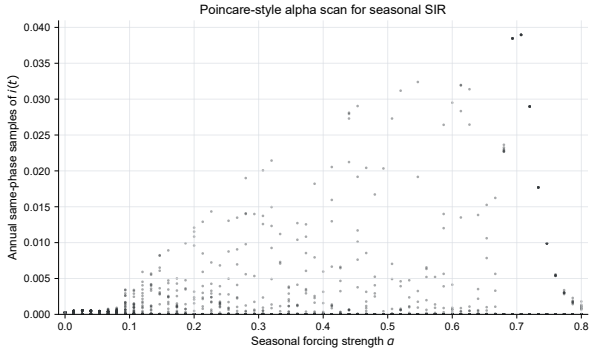

(a) Annual samples after transient removal become more dispersed as forcing strength increases, suggesting changes in long-run structure.

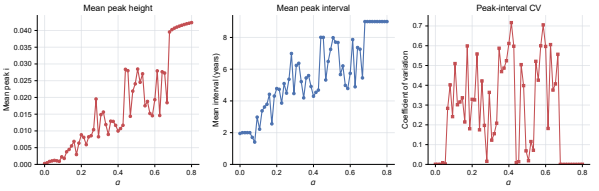

(b) Peak height, peak interval, and peak-interval variability change with α, supporting the regime differences seen in the scan.

Figure 8: Seasonal alpha-scan diagnostics based on annual sampling and detected infection peaks.

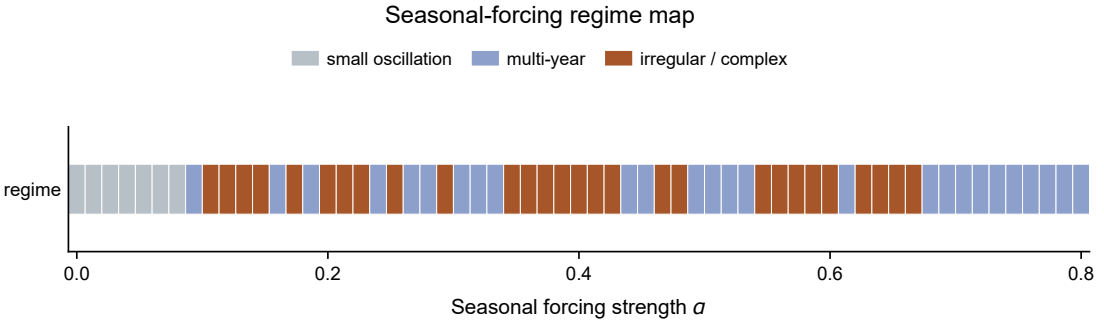

Figure 9: Numerical regime map for the seasonal forcing scan. The classification summarizes small oscillations, multi-year cycles, and irregular or complex patterns, but should be understood as a numerical diagnostic rather than a strict bifurcation proof.

Table 4 reports representative alpha values from the scan. The table should be read together with the two diagnostic figures: the annual samples describe the long-run state once per forcing period, while the peak statistics summarize the detected bursts between those samples. Neither diagnostic alone is sufficient for a rigorous classification, but together they provide a stable numerical description of how the forcing strength changes the observed outbreak pattern. At $\alpha = 0$, the mean peak height is only about 2.62×10^{-4} and the relative variation of peak intervals is negligible. At $\alpha = 0.2$, 0.4, and 0.6, the numerical classification indicates irregular or complex oscillation, with higher peak-height and peak-interval variability. At $\alpha = 0.8$, the mean peak interval is about 9.00 years and the coefficients of variation are very small, consistent with a regular multi-year pattern in the numerical scan. Here CV denotes coefficient of variation, so a smaller CV indicates more regular peak heights or intervals within the detected long-run window.

Table 4
Representative seasonal forcing summary. Pattern labels are numerical diagnostics based on long-run annual samples and detected peaks; CV denotes coefficient of variation.

α	Diagnostic pattern	Peaks	Mean peak i	Mean interval (yr)	Peak-height CV
0.0	small oscillation	19	2.62×10^{-4}	1.95	0.022
0.2	irregular / complex	12	8.83×10^{-3}	4.78	0.509
0.4	irregular / complex	14	9.97×10^{-3}	4.30	0.735
0.6	irregular / complex	9	1.93×10^{-2}	5.74	0.593
0.8	multi-year	7	4.24×10^{-2}	9.00	0.0019

The mathematical role of α is also visible from the growth inequality

$$\beta_0\{1 + \alpha\cos(2\pi t)\}s(t) > \gamma + \mu. \tag{47}$$

Increasing α widens the gap between favorable and unfavorable parts of the year. During favorable phases, the threshold susceptible level for growth is lower; during unfavorable phases, the threshold becomes higher. Therefore stronger seasonal forcing can create separated infection bursts even when the mean transmission level is fixed. The numerical pattern labels in Table 4 should be interpreted through this inequality: they summarize how the periodic growth window interacts with susceptible replenishment over many years.

These results show that seasonal forcing provides a minimal external mechanism for sustained long-term recurrent outbreaks. The model does not merely create another initial transient peak; after transient removal, the infection curve can retain repeated pulse-like structures whose timing and amplitude depend on the forcing strength.

4.4. Stochastic effects: why do small infected counts matter?

The stochastic experiments examine how integer infected counts alter outbreak outcomes. Figure 10 compares repeated stochastic trajectories with the deterministic demographic curve. During the early outbreak, the stochastic paths follow the deterministic wave closely when $N = 10000$ and $I_0 = 20$. However, after the epidemic wave, the finite stochastic system reaches $I = 0$, which is absorbing. This is why the establishment experiments focus on early fade-out before a major outbreak threshold is reached, rather than interpreting all eventual disease disappearance as the same event.

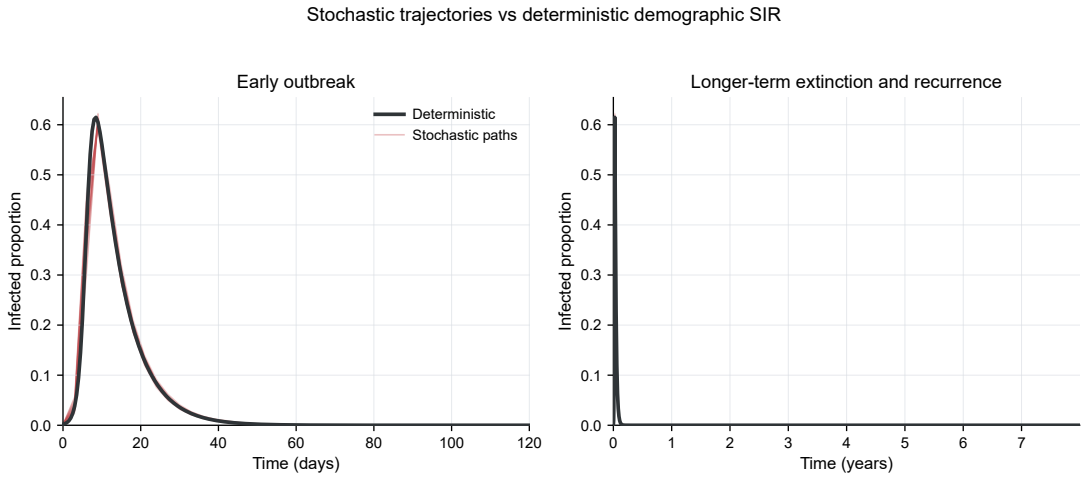

Figure 10: Stochastic trajectories and the deterministic demographic curve. Large early outbreaks are close to the deterministic wave, but the finite stochastic process can eventually hit the absorbing state $I = 0$.

Figure 11 summarizes near-threshold establishment experiments. The heatmap shows early fade-out probability across population size and initial infected count. For fixed population size, increasing I_0 generally reduces early

fade-out because a larger infection seed is less likely to be removed by the first few recovery or death events. For fixed I_0, larger population size does not automatically reduce early fade-out in this design because the major-outbreak threshold is proportional to N, so a larger absolute number of infections is required for establishment. The fade-out time distribution also becomes wider for larger N, indicating that some failed establishments can persist longer before disappearance.

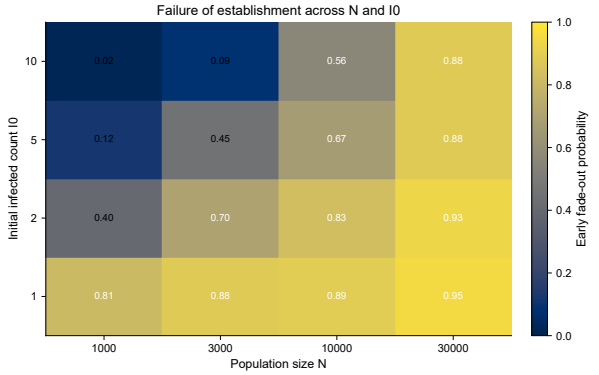

(a) Early fade-out probability decreases with larger I_0 in small populations, but threshold scaling makes the dependence on N non-monotone.

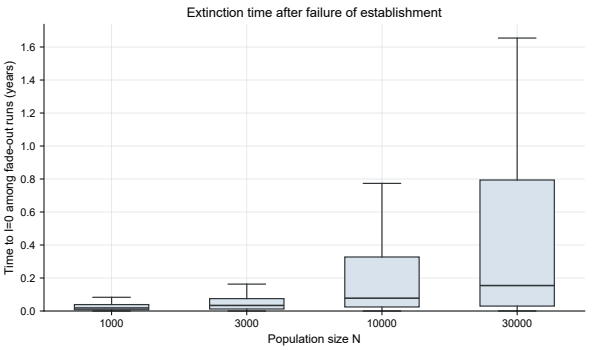

(b) Fade-out times are more spread out for larger populations, showing that failed establishment can last for different durations.

Figure 11: Near-threshold stochastic establishment diagnostics.

Seasonal stochastic experiments further show that forcing strength and initial seasonal phase affect establishment risk. Figure 12 shows that, under phase-0 initialization, increasing α from 0 to 0.6 reduces early fade-out probability from about 0.69 to about 0.05. This conclusion is phase-dependent. Figure 12b shows that for the same α, starting at phase $\pi/2$ or phase π can lead to much higher early fade-out probability. Hence seasonal forcing can help establishment when the initial infected individuals appear during a favorable transmission phase, but it can also suppress establishment under an unfavorable phase.

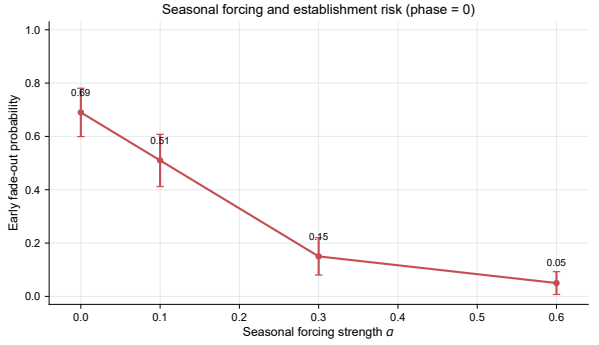

(a) Under phase-0 initialization, stronger seasonal forcing lowers early fade-out probability and increases establishment probability.

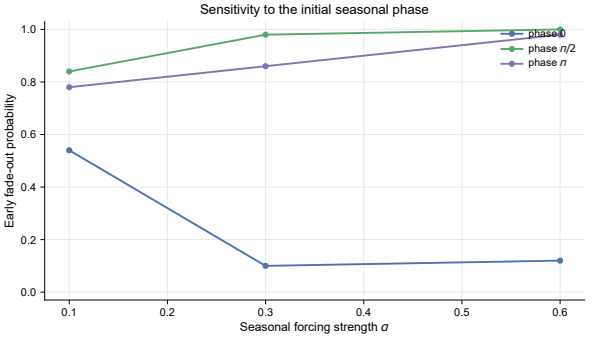

(b) The seasonal alpha effect is sensitive to the initial phase; unfavorable phases can produce high early fade-out even at large α.

Figure 12: Seasonal stochastic establishment under different forcing strengths and initial phases.

Table 5 gives representative stochastic summaries. The rows with $N = 1000$ show a strong effect of I_0: early fade-out probability decreases from 0.81 at $I_0 = 1$ to 0.02 at $I_0 = 10$. Under the phase-0 seasonal alpha scan with $N = 10000$ and $I_0 = 5$, early fade-out probability decreases from 0.69 at $\alpha = 0$ to 0.05 at $\alpha = 0.6$. This numerical

trend is consistent with Figure 12a, but Figure 12b shows that it should not be generalized without specifying the initial seasonal phase.

Table 5
Representative stochastic early fade-out summary. A major outbreak is counted only if the infected count reaches the threshold shown in the table; otherwise the run is counted as early fade-out.

Scenario	N	I_0	α	Threshold	Fade-out prob.	Major prob.	Median fade-out time
Near-threshold	1000	1	0	5	0.81	0.19	0.0117
Near-threshold	1000	5	0	6	0.12	0.88	0.0363
Near-threshold	1000	10	0	11	0.02	0.98	0.1199
Near-threshold	10000	1	0	50	0.89	0.11	0.0232
Near-threshold	10000	5	0	50	0.67	0.33	0.1949
Near-threshold	30000	5	0	150	0.88	0.12	0.5941
Seasonal phase 0	10000	5	0.0	50	0.69	0.31	0.2567
Seasonal phase 0	10000	5	0.3	50	0.15	0.85	0.0605
Seasonal phase 0	10000	5	0.6	50	0.05	0.95	0.0426

The stochastic establishment probabilities can be interpreted through the competition between the first few infection events and the first few removal events. When I is small, the infection rate is approximately proportional to I and the recovery/death rates are also proportional to I:

$$a_1(t) \approx \beta(t) s I, \qquad a_2(t) + a_3(t) \approx (\gamma + \mu) I. \tag{48}$$

The ratio

$$\frac{a_1(t)}{a_2(t) + a_3(t)} \approx \frac{\beta(t) s}{\gamma + \mu} = \mathcal{R}_{\text{eff}}(t) \tag{49}$$

indicates the expected local advantage of infection over removal. However, when I is only one or a few individuals, this ratio is not enough to guarantee survival. Random ordering matters: if removals occur before enough infections accumulate, the process reaches $I = 0$ and the outbreak fails to establish.

Overall, the stochastic results answer the optional question: small infected counts matter because demographic and seasonal growth tendencies do not guarantee establishment in a finite population. In practical interpretation, the stochastic layer should therefore be viewed as an establishment filter placed before the deterministic epidemic wave. Even when the deterministic growth condition is favorable, a few recovery or death events can remove the infection before it crosses the major-outbreak threshold.

5. Discussion

The four model layers provide complementary explanations for periodic epidemic behavior. First, the basic SIR model explains a single epidemic wave through threshold growth and susceptible depletion. Its long-term disappearance of infection is not a numerical accident; it follows from the lack of new susceptible input. Second, demographic turnover creates a slow susceptible-replenishment mechanism. This can generate recurrent peaks, especially at higher transmission levels, but these peaks are not necessarily externally synchronized. Third, seasonal forcing supplies an explicit periodic driver. The alpha-scan results show that forcing strength changes the long-run infection pattern, with weak forcing producing small oscillations, intermediate forcing producing more variable recurrent bursts, and high forcing producing multi-year regularity in part of the scan. Fourth, stochasticity explains why finite infected counts can fail to establish despite favorable deterministic conditions.

Several limitations should be kept in mind. The models assume homogeneous mixing and do not include age structure, spatial heterogeneity, contact networks, vaccination, or behavior change. The seasonal forcing is represented by a single cosine term, which is a deliberately simplified description of periodic transmission variation. The regime classification in the seasonal scan is a numerical diagnostic based on annual samples and detected peaks, not a rigorous

mathematical bifurcation theorem. The stochastic establishment results also depend on the selected threshold, the initial susceptible count, and the initial seasonal phase. In particular, the phase-0 trend in Figure 12a should be interpreted together with the phase-sensitivity result in Figure 12b.

These limitations do not undermine the mechanism exploration objective. A simplified model can still be informative when each added mechanism has a clear interpretation and a visible numerical consequence. In this report, every additional assumption is tested against a specific question: whether it changes one outbreak into recurrence, whether it organizes recurrence into long-term periodicity, or whether it prevents establishment at small counts. Instead, they clarify the role of each modeling assumption. The minimal deterministic mechanism for sustained recurrent outbreaks in this experiment is not the basic SIR model alone, but the combination of susceptible replenishment and periodic transmission forcing. The stochastic model then adds a separate finite-population layer: the deterministic mechanism describes expected growth tendencies, while stochastic fade-out determines whether a small initial infection actually becomes established.

6. Conclusion

This report investigated periodic outbreak formation through a sequence of SIR-type models. The basic SIR model produces a single outbreak because susceptible depletion eventually forces the infected proportion to decay toward zero. Adding demographic turnover replenishes susceptible individuals and can produce recurrent late peaks, especially under high transmission. Introducing seasonal forcing creates a minimal external periodic driver and leads to long-term recurrent structures whose peak heights, intervals, and diagnostic regimes vary with the forcing strength. Finally, stochastic simulations show that small infected counts can lead to early fade-out before a major outbreak is established, and that the seasonal effect on establishment risk depends strongly on the initial phase.

The modeling evidence also suggests a practical hierarchy of mechanisms. Transmission and recovery determine whether the first wave can grow; susceptible replenishment determines whether later waves can reappear; seasonal forcing determines whether those later waves are organized by an external calendar-like driver; and finite-population randomness determines whether a small infection seed can survive long enough for the deterministic tendency to become visible. This hierarchy is useful because it prevents over-interpreting a single curve: a large first peak, a late recurrent peak, a multi-year seasonal pattern, and a failed stochastic establishment event correspond to different mathematical mechanisms.

From an experimental perspective, the value of the model sequence lies in the consistency between equations, figures, and summary tables. The threshold scan matches the analytic growth condition, the demographic summaries quantify secondary peaks, the seasonal scan records changes in long-run recurrence, and the stochastic summaries quantify failure of establishment. The complete experiment chain supports a clear modeling conclusion: persistent periodic outbreaks require more than the basic SIR depletion mechanism. Susceptible replenishment makes recurrence possible, seasonal transmission can organize sustained periodic dynamics, and finite-population stochasticity determines whether low-count infections survive long enough to enter the deterministic outbreak regime.